Dalton Transactions

ROYAL SOCIETY OF CHEMISTRY

PAPER

View Article Online
View Journal | View Issue

Check for updates

Cite this: *Dalton Trans.*, 2020, **49**, 3450

Increased photocurrent of $CuWO_4$ photoanodes by modification with the oxide carbodiimide $Sn_2O(NCN)$†

Zheng Chen,[a] Manuel Löber,[b] Anna Rokicińska,[c] Zili Ma,[a] Jianhong Chen,[d] Piotr Kuśtrowski,[c] Hans-Jürgen Meyer,[b] Richard Dronskowski[a,e] and Adam Slabon*[d]

Tin(II) oxide carbodiimide is a novel prospective semiconductor material with a band gap of 2.1 eV and lies chemically between metal oxides and metal carbodiimides. We report on the photochemical properties of this oxide carbodiimide and apply the material to form a heterojunction with $CuWO_4$ thin films for photoelectrochemical (PEC) water oxidation. Mott–Schottky experiments reveal that the title compound is an n-type semiconductor with a flat-band potential of −0.03 V and, as such, the position of the valence band edge would be suitable for photochemical water oxidation. $Sn_2O(NCN)$ increases the photocurrent of $CuWO_4$ thin films from 32 μA cm^{-2} to 59 μA cm^{-2} at 1.23 V *vs.* reversible hydrogen electrode (RHE) in 0.1 M phosphate buffer (pH 7.0) under backlight AM 1.5G illumination. This upsurge in photocurrent originates in a synergistic effect between the oxide and oxide carbodiimide, because the heterojunction photoanode displays a higher current density than the sum of its individual components. Structural analysis by powder X-ray diffraction (XRD) and X-ray photoelectron spectroscopy (XPS) reveals that $Sn_2O(NCN)$ forms a core–shell structure $Sn_2O(NCN)@SnPO_x$ during the PEC water oxidation in phosphate buffer. The electrochemical activation is similar to the behavior of Mn(NCN) but different from Co(NCN).

Received 14th December 2019,
Accepted 17th February 2020

DOI: 10.1039/c9dt04752b

rsc.li/dalton

This article is licensed under a Creative Commons Attribution 3.0 Unported Licence.

Introduction

One of the critical technical problems facing humanity is the development of a long-term sustainable energy economy.[1] This especially includes clean and renewable energy generation; a task that can be theoretically fulfilled by photoelectrochemical (PEC) water-splitting to yield hydrogen.[2] Water-splitting consists of two half reactions: the transfer of two electrons for the hydrogen evolution reaction (HER) and four electrons for the oxygen evolution reaction (OER).[3] The photo-generated charge and holes separate and migrate through the semiconductor in opposite directions to generate a photocurrent. Since the initial report on solar-driven water-splitting on a TiO_2 photoelectrode in 1972,[4] metal oxide semiconductors have been intensively investigated, and $BiVO_4$ has emerged as the benchmark oxide photoanode.[5] There are only few known oxidic photoanode candidates that display a smaller band gap than $BiVO_4$, such as $CuWO_4$ with an electronic band gap in the range of 2.2–2.4 eV.[6]

There are several critical characteristics for a semiconductor material in terms of realistic application as a water-splitting photoelectrode: (i) suitable conduction and/or valence band edge positions; (ii) stability under operating conditions; (iii) efficient charge carrier separation and transport along and across the thin-film electrode; (iv) low-cost and earth-abundant elements; and (v) sufficient light absorption.[5–7] Additionally, the surface of the light absorber has to be modified in most cases with a suitable catalyst to overcome poor reaction kinetics, *i.e.* to drive the HER and/or OER.[8]

Copper tungstate is one of the few promising photoanode materials with a suitable band gap, a valence band edge (VBE) more positive than 1.23 V *vs.* RHE to permit water oxidation, stability under neutral conditions and composed of abundant elements.[9] It can be manufactured on differential electrically conductive substrates by electrochemical deposition,[10] atomic layer deposition (ALD),[11] spray pyrolysis,[12] and spin-casting.[13] Several strategies have been reported to improve the perform-

[a]*Chair of Solid-State and Quantum Chemistry, Institute of Inorganic Chemistry, RWTH Aachen University, 52056 Aachen, Germany*
[b]*Section of Solid State and Theoretical Inorganic Chemistry, Institute of Inorganic Chemistry, University of Tübingen, 72076 Tübingen, Germany*
[c]*Faculty of Chemistry, Jagiellonian University, 30-387 Krakow, Poland*
[d]*Department of Materials and Environmental Chemistry, Stockholm University, 10691 Stockholm, Sweden. E-mail: adam.slabon@mmk.su.se*
[e]*Hoffmann Institute of Advanced Materials, Shenzhen Polytechnic, 7098 Liuxian Blvd, Shenzhen, China*

†Electronic supplementary information (ESI) available. See DOI: 10.1039/c9dt04752b

This journal is © The Royal Society of Chemistry 2020

This article is licensed under a Creative Commons Attribution 3.0 Unported Licence.

ance of $CuWO_4$ by doping with zinc,[14] molybdenum[15] or iron,[12] incorporating with silver nanowires,[16] functionalizing with gold nanoparticles.[17] Charge transport is also facilitated by post-synthetic hydrogen or nitrogen treatment of $CuWO_4$ due to the formation of oxygen vacancies.[10,18] Recently, we have reported that surface modification of $CuWO_4$ with $Ag_2(NCN)$[8a] or Mn(NCN)[8b] displays synergetic effects between its constituents, which improve PEC water oxidation efficiency.

Carbodiimides have received attention as novel materials for photochemical energy conversion in addition to their application as electrode materials for Li-ion batteries.[19] This has been mainly motivated by their suitable band gap values for solar light harvesting and a beneficial VBE position for PEC water oxidation.[20] They are related to oxides but are characterized by a higher degree of covalency.[21] The carbodiimide anion ($^{-}N{=}C{=}N^{-}$) is considered as a pseudo-chalcogenide anion and lies between oxide and sulfide anions in view of the HSAB concept.[22] The oxide carbodiimides are as such mixed-anion compounds. The oxide carbodiimide representative $Sn_2O(NCN)$ was obtained recently by Meyer *et al.* as crystalline powder with an optical band gap of approximately 2.0 eV.[23] The title compound is closely related to tin(II) oxide (SnO); a semiconductor with a band gap of 2.8 eV as calculated on the basis of electronic band structure calculations.[24]

In this work, we report on the photochemical properties of $Sn_2O(NCN)$ and the fabrication of heterojunction $CuWO_4/Sn_2O(NCN)$ thin film photoanodes. We show that $Sn_2O(NCN)$ undergoes structural changes during PEC water oxidation and can augment the photocurrent of $CuWO_4$ photoanodes.

Experimental

Synthesis of $Sn_2O(NCN)$

$Li_2(NCN)$ was prepared as previously reported by Meyer.[23,25] Equimolar amounts of $Li_2(NCN)$, Na_2O and $SnCl_2$ (Sigma Aldrich 99.999%, ultra dry) were mixed and ground in an agate mortar under argon. Samples of 250 mg were sealed into silica tubes under vacuum and each mixture was heated in a furnace to temperatures ranging from 450 to 500 °C. The samples were kept for 12 h before cooling to room temperature. The ampoules were opened in air, the product was washed with deionized water and dried in oven at 80 °C for 4 h. $Sn_2O(NCN)$ was obtained as a red powder.

Synthesis of $CuWO_4$ thin films

$CuWO_4$ thin films were produced on conductive fluorine-doped tin oxide (FTO) glass (2.0 mm thick, Sigma-Aldrich), based on a synthesis by Bartlett.[9a] Before the electrochemical synthesis, the FTO glass was cleaned in diluted nitric acid (Sigma), acetone and ethanol, respectively. 1.26 g (3.8 mmol) sodium tungstate dihydrate ($Na_2WO_4{\cdot}2H_2O$, 99.9%, Acros Organics) was dissolved in 15 mL deionized water by stirring, and 1 mL hydrogen peroxide (30%, Geyer Chemsolute) was added to the tungstate precursor solution. The solution was stirred for 20 min at room temperature. 25 mL deionized water and 25 mL isopropanol (>99.7%, Fisher Scientific) were added to the solution. A solution of 0.73 g (2.7 mmol) copper(II) nitrate trihydrate ($Cu(NO_3)_2{\cdot}3H_2O$, >99%, Sigma) in 10 mL deionized water was added to the tungsten precursor solution. The pH value was adjusted to 1.2 by adding nitric acid and the solution was used for electrochemical deposition on FTO glass. The electrochemical deposition was performed in a three-electrode setup with platinum wire and 1 M Ag/AgCl (WAT Venture) as a counter electrode and a reference electrode, respectively. The electrochemical deposition was carried out by a Gamry potentiostat and the Gamry framework software package. The potential was swept in the range from −0.9 to +0.2 V *vs.* 1 M Ag/AgCl for 12 cycles at the scan rate of 50 mV s^{-1}. The working electrode was disconnected in the electrical circuit, washed with deionized water and dried at room temperature under vacuum. The working electrode was heated at 450 °C for 2 h under ambient atmosphere. The excess of copper oxides was etched by immersing the working electrode into 0.5 M HCl for acidic treatment. The electrode was subsequently annealed one more time at 450 °C for 30 min under ambient atmosphere.

Preparation of $Sn_2O(NCN)$ and $CuWO_4/Sn_2O(NCN)$ photoanodes

$Sn_2O(NCN)$ powder was dispersed in ethanol (120 μg mL^{-1}) by ultrasounds. FTO, a bare graphite (for XPS) and $CuWO_4$ thin film electrode were placed on a heating plate at 50 °C. The $Sn_2O(NCN)$ dispersion was drop-casted on the surfaces of the corresponding thin film electrodes.

Structural characterization

Powder XRD patterns were recorded in transmission mode on a STOE STADI-P diffractometer (Cu $K_{\alpha1}$ radiation) operating with a DECTRIS Mythen 1K detector. For the analysis of the photoanodes by XRD, the samples were mechanically removed from the photoanodes in advance. SEM images of $Sn_2O(NCN)$ powder were recorded by a Leo Supra 35VP SMT (Zeiss).

A Themis Z TEM (Thermo Fisher) equipped with a SuperX energy dispersive X-ray (EDX) detector operated at 300 kV in the scanning TEM mode was used for determination of the chemical composition of $Sn_2O(NCN)$ particles, which were subject to chronoamperometry at 1.23 V *vs.* RHE. Prior to the analysis, the particles were mechanically removed from the pure $Sn_2O(NCN)$ electrode.

XPS spectra were collected by a hemispherical VG SCIENTA R3000 analyzer using a monochromatized aluminum source Al K_α (E = 1486.6 eV) at constant pass energy of 100 eV. The binding energies were referenced to the Au 4f core level (E_b = 84.0 eV). The composition and chemical surrounding of the sample surface were determined on the basis of the areas and binding energies of Na 1s, K 2p, P 2p, O 1s, N 1s, C 1s and Sn 3d photoelectron peaks. The fitting of high resolution spectra was obtained by using the Casa XPS software. UV-Vis spectra were recorded on a Shimadzu UV-2600 spectrophotometer. Measurements were recorded in absorbance and reflectance

This article is licensed under a Creative Commons Attribution 3.0 Unported Licence.

mode. The Tauc plots were calculated by Kubelka–Munk function $F(R) = (1 - R)^2/2R$ to determine the electronic band gap.

Photoelectrochemistry

The experiments were carried out in an electrochemical cell operating in a three-electrode setup. The photoanode was used as a working electrode. Platinum wire and a 1 M Ag/AgCl electrode were used as a counter electrode and a reference electrode, respectively. All current values of the electrodes were recorded *vs.* 1 M Ag/AgCl reference electrode and converted *vs.* RHE according to E_{RHE} (V) = $E_{1\ M\ Ag/AgCl}$ (V) + 0.236 (V) + [0.059 × pH] (V) at 25 °C. The electrochemical data were recorded by a potentiostat (Gamry instruments). A solar light simulator (class-AAA 94023A, Newport) with an ozone-free 450 W xenon short-arc lamp was used to illuminate the photoanode with 100 mW cm^{-2} (AM 1.5G) simulated visible light. The power output of the solar simulator was calibrated with a Si reference cell (LOT-Quantum Design, Germany). 0.1 M potassium/sodium phosphate (K/NaP_i) buffer (or with 0.05 M Na_2SO_3 as hole scavenger) at pH 7.0 was used as the electrolyte for PEC experiments and prepared with Milli-Q water (18.3 Ω cm) at 25 °C. The linear square voltammetry (LSV) and cyclic voltammetry (CV) were swept at a scan rate of 10 mV s^{-1} from 0.64 to 1.44 V *vs.* RHE. Mott–Schottky (MS) measurements were carried out under dark in an electromagnetically shielded box. A sinusoidal modulation of 10 mV was applied at frequencies of 10 Hz, 100 Hz and 1000 Hz in the potential range from 0.05 V to 1.23 V *vs.* RHE with an equilibration time of 10 s.

Results and discussion

Structure characterization of the bulk

Fig. 1a shows SEM images of the obtained microcrystalline $Sn_2O(NCN)$ and the thin film $CuWO_4/Sn_2O(NCN)$ photoanode. $Sn_2O(NCN)$ crystallizes in an orthorhombic crystal structure (space group *Pccn*) and has Sn^{2+} ions situated in a fourfold, mixed O^{2-}/NCN^{2-} coordination environment.[23] The carbodiimide anion is closely related to the oxide anion and can be regarded as an N-based pseudo-oxide.[26] For structural characterization, we tested the photoanodes for PEC water oxidation (*vide infra*) and removed subsequently a part of the thin film for XRD and XPS characterization. The powder XRD patterns of a pure $Sn_2O(NCN)$ photoanode indicate that the compound maintains its structural bulk stability after PEC water oxidation in phosphate electrolyte at pH 7.0 (Fig. 2).

The corresponding powder XRD patterns of the composite $CuWO_4/Sn_2O(NCN)$ photoanodes do not exhibit reflection peaks of the oxide carbodiimide due to the low amount of the latter (Fig. 3). The XRD patterns before and after PEC operation remain unchanged and match the simulated patterns of the copper tungstate.

Electronic structure

The electronic band gaps of $CuWO_4$ and $Sn_2O(NCN)$ were determined by the Kubelka–Munk function. The results show

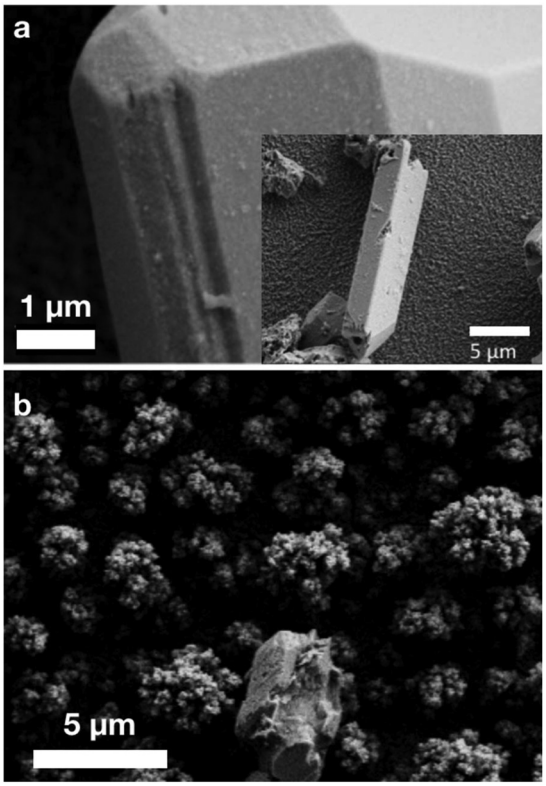

Fig. 1 SEM micrographs of (a) $Sn_2O(NCN)$ and (b) thin film photoanode $CuWO_4/Sn_2O(NCN)$. The latter contains the continuous $CuWO_4$ thin film on which the rectangular-shaped $Sn_2O(NCN)$ particle is deposited (bottom).

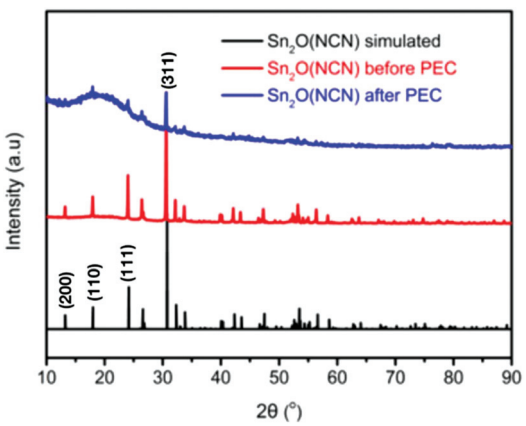

Fig. 2 Experimental and simulated powder XRD patterns of $Sn_2O(NCN)$ before and after PEC water oxidation. The reflection peaks (310), (400) and (211) overlap between (111) and (311) and are not marked in the patterns.

that the band gap of $CuWO_4$ and $Sn_2O(NCN)$ are 2.31 and 2.10 eV, respectively (Fig. 4). Both determined values are close to the previously reported values of 2.2–2.4 eV for $CuWO_4$[14] and 2.0 eV for $Sn_2O(NCN)$.[23] This would render both compounds as potential photoanode candidates for water oxidation.

 This journal is © The Royal Society of Chemistry 2020

This article is licensed under a Creative Commons Attribution 3.0 Unported Licence.

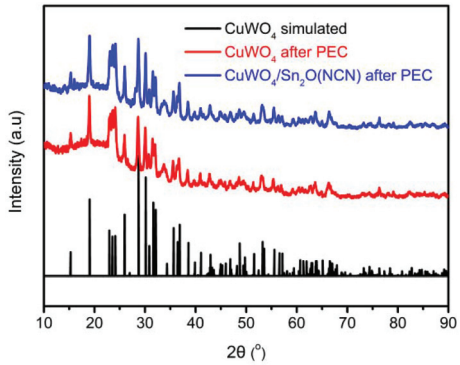

Fig. 3 Experimental and simulated powder XRD patterns of $CuWO_4$ and $CuWO_4/Sn_2O(NCN)$ after PEC water oxidation.

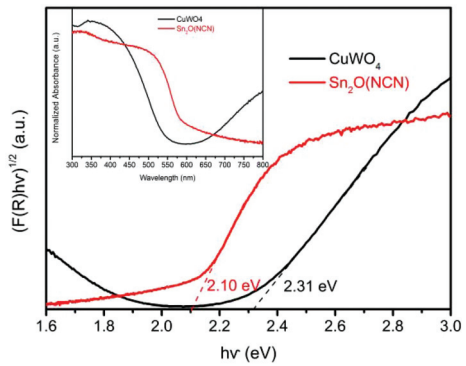

Fig. 4 Tauc plots for $Sn_2O(NCN)$ and $CuWO_4$. The inset shows the normalized absorbance spectra.

The semiconducting type and band edge positions of $Sn_2O(NCN)$ were determined by MS measurements. Fig. 5 illustrates the MS plots of $Sn_2O(NCN)$ photoanodes for applied different frequencies of 10, 100 and 1000 Hz. All curves exhibit a positive slope, indicating that the oxide carbodiimide $Sn_2O(NCN)$ is an n-type semiconductor; similar to $CuWO_4$. For all three different frequencies, extrapolation of the measured data yields a flat-band potential of −0.03 V *vs.* RHE. For an n-type semiconductor, the value of the flat-band potential is close to the conduction band edge (CBE) position. Taking into account the determined band gap, the VBE and CBE positions are 2.07 V and −0.03 V *vs.* RHE, respectively. A comparison of the CBE and VBE positions for the binary tin oxides is shown in Fig. S1.† Similar to SnO_2, the oxide carbodiimide would be theoretically suited for overall water-splitting.[24,27]

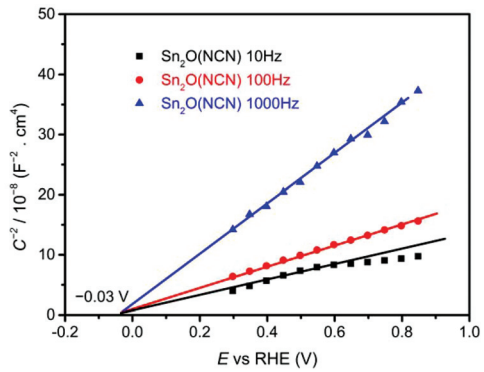

Fig. 5 MS analysis of EIS measurements of $Sn_2O(NCN)$ electrodes applied frequencies of 10, 100 and 1000 Hz.

Photoelectrochemistry

For the investigation of heterojunction photoanodes $CuWO_4/Sn_2O(NCN)$, two additional electrodes of the individual components were produced. All measurements were performed in phosphate electrolyte at pH 7.0. The summarized LSV curves for all three electrodes, recorded with a scan rate at 10 mV s^{-1} under backlight AM 1.5G illumination (100 mW cm^{-2}), are depicted in Fig. 6. The $CuWO_4$ photoanode developed an anodic current that reached 32 μA cm^{-2} at 1.23 V *vs.* RHE.

Upon functionalizing the surface with $Sn_2O(NCN)$ particles by drop-casting, the photocurrent showed an upsurge which was reached when adding 36 μg (Fig. S2†). A bare $Sn_2O(NCN)$ electrode with the same amount of material as for the composite photoanode $CuWO_4/Sn_2O(NCN)$ developed only a small photocurrent. The photocurrent produced by the heterojunction electrode, being equal 59 μA cm^{-2} at 1.23 V *vs.* RHE, exceeds the sum of its individual components and exhibits as such a synergistic effect. This trend is more visible during chronoamperometry (CA) with interrupted illumination (Fig. 7). The photocurrent remains relatively stable for a tested period of 2 hours (Fig. S3†).

Since the photocurrent of the oxide carbodiimide was very small, we created another $Sn_2O(NCN)$ photoanode by electrophoretic deposition with a higher amount of material. Fig. 8 illustrates the results of CA for this $Sn_2O(NCN)$ photoanode and FTO glass, as a reference measurement, at 1.23 V *vs.* RHE in the same electrolyte under illumination. It can be clearly seen that the photocurrent of $Sn_2O(NCN)$ outperforms the substrate. As such one can rule out that the photoactivity of $Sn_2O(NCN)$ may be due to surface oxidation toward a tin oxide phase.

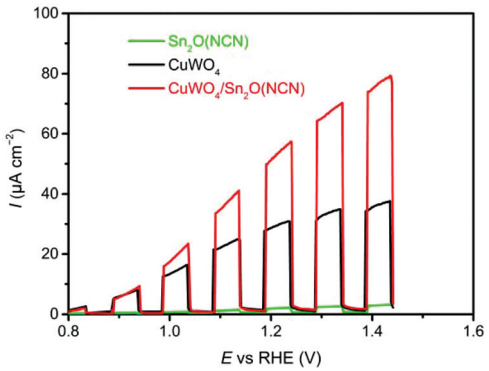

Fig. 6 LSV of $Sn_2O(NCN)$, $CuWO_4$ and $CuWO_4/Sn_2O(NCN)$ photoanodes. Measurements were performed in 0.1 M phosphate electrolyte (pH 7.0) with scan at rate of 10 mV s^{-1} under sequentially interrupted backlight AM 1.5G illumination (100 mW cm^{-2}).

This article is licensed under a Creative Commons Attribution 3.0 Unported Licence.

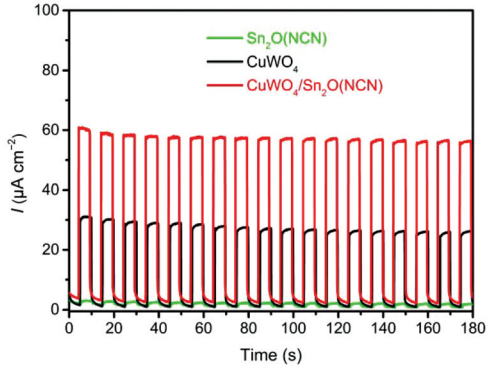

Fig. 7 CA of $Sn_2O(NCN)$, $CuWO_4$ and $CuWO_4/Sn_2O(NCN)$ photoanodes at 1.23 V *vs.* RHE. Measurements were performed in 0.1 M K phosphate electrolyte (pH 7.0) under sequentially interrupted backlight AM 1.5G illumination (100 mW cm^{-2}).

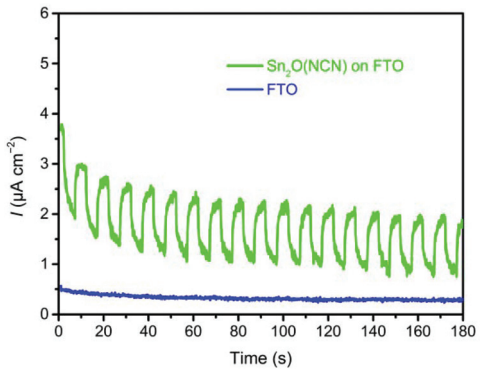

Fig. 8 CA of bare $Sn_2O(NCN)$ and the FTO substrate at 1.23 V *vs.* RHE. Measurements were performed in 0.1 M phosphate electrolyte (pH 7.0) under sequentially interrupted backlight AM 1.5G illumination (100 mW cm^{-2}).

In order to elucidate the origin of increased photocurrents after $Sn_2O(NCN)$ functionalization, we determined the hole collection efficiency η_{hc}. The oxidation of a hole scavenger, such as the sulfite anion, allows to determine the number of surface-reaching holes because this oxidation reaction is much faster than the sluggish oxidation of water. This allows to estimate that each hole reaching the semiconductor–electrolyte interface will be used for an oxidative reaction. The comparison of the photocurrents for sulfite oxidation ($J_{Na_2SO_3}$) and water oxidation (J_{H_2O}) allows to calculate $\eta_{hc} = (J_{H_2O}/J_{Na_2SO_3})$. For the $CuWO_4$ thin films, the η_{hc} value significantly increases upon functionalization with $Sn_2O(NCN)$ at higher potentials (Fig. 9). This indicates that the reactivity of the surface increases upon functionalization with the oxide carbodiimide.

To investigate the key factors of improved PEC performance, we analyzed the surface of bare $Sn_2O(NCN)$ photoanodes after the PEC experiment by XPS. The electrode was prepared on graphite instead of FTO substrate to avoid interference with Sn stemming from FTO. Except the presence of O, C, N and Sn, XPS reveals the presence of Na, K and P which originate

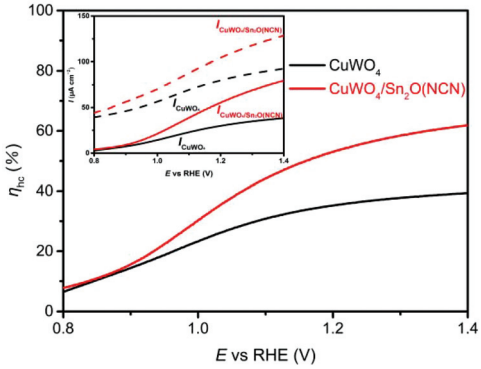

Fig. 9 Hole collection efficiencies η_{hc} of $CuWO_4$ and $CuWO_4/Sn_2O$ (NCN) photoanodes. The inset shows the photocurrent densities during water (solid line) and sulfite oxidation (dashed line) for $CuWO_4$ (black) and $CuWO_4/Sn_2O(NCN)$ (red) photoanodes.

from the K/NaP_i electrolyte. In Fig. 10, the high-resolution XPS Sn 3d spectrum, with the Sn $3d_{5/2}$ and Sn $3d_{3/2}$ peaks distanced at the splitting energy of 8.4 eV, is shown. The latter one is partially overlapped with the Na KLL Auger signal. The relative high values of binding energies found for both components (487.5 eV for Sn $3d_{5/2}$ and 495.9 eV for Sn $3d_{3/2}$) obviously suggest that $Sn_2O(NCN)$ formed a phosphate-type shell on the surface being exposed to the phosphate electrolyte, *i.e.* a core–shell structure $Sn_2O(NCN)@SnPO_x$. This indicates that the catalytically active form is a tin phosphate shell while the core contains the semiconducting $Sn_2O(NCN)$. Similar positions of the Sn 3d signals have been observed recently for tin phosphate ($SnPO_x$) in relation to SnO_2, which exhibited the Sn $3d_{5/2}$ and Sn $3d_{3/2}$ components at 486.0 eV and 494.4 eV, respectively.[28] Different from the behavior of Co (NCN) electrocatalysts,[29] the electrochemical activation is similar to the behavior of Mn(NCN) electrocatalysts[8b] as previously reported. Tin phosphate is known as a heterogeneous catalyst for efficient dehydration of glucose into 5-hydroxymethylfurfural in ionic liquid according to the literature

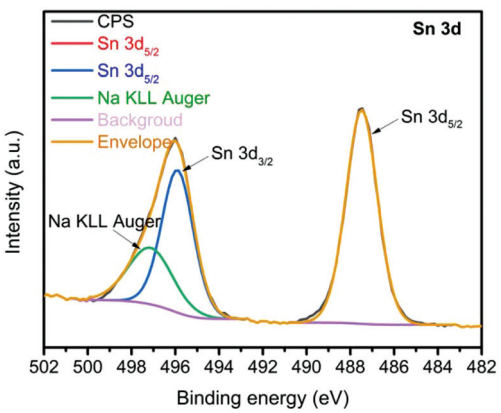

Fig. 10 XPS Sn 3d spectrum of bare $Sn_2O(NCN)$ on graphite after PEC water oxidation.

This journal is © The Royal Society of Chemistry 2020

This article is licensed under a Creative Commons Attribution 3.0 Unported Licence.

report. The fourfold coordinated Sn^{4+} sites from tin phosphate are identified as the active species.[28]

The presence of phosphorous was also confirmed by complementary TEM EDX analysis, which was performed on Sn_2O (NCN) particles that were mechanically removed from a FTO/Sn_2O(NCN) thin film electrode after 30 min of CA at 1.23 V *vs.* RHE. The high-angle annular dark field (HAADF) images in Fig. 11 shows agglomerated particles that were scanned by means of EDX. Besides phosphorous, the presence of tin, oxygen, carbon and nitrogen could be confirmed, too.

The augmented charge carrier separation for the heterojunction can be understood by analyzing the energy band diagram of both semiconductors (Fig. 12).[8a] The energetically higher position of the CBE for Sn_2O(NCN) in comparison to $CuWO_4$ enables injection of electrons into the conduction band of the latter. At the same time, the photogenerated holes can diffuse from the VBE of $CuWO_4$ to Sn_2O(NCN). This results in decreased recombination of photogenerated electrons and holes. In addition to the improved hole collection efficiency, being the consequence of the tin phosphate shell, the PEC water oxidation efficiency could be further increased by 10% when depositing cobalt phosphate as co-catalyst on the surface of the heterojunction photoanode (Fig. S4†).

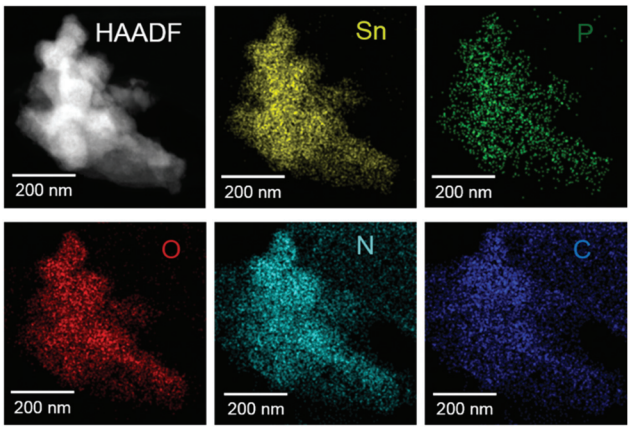

Fig. 11 HAADF image and corresponding elemental maps of Sn_2O (NCN) particles that were subject to CA at 1.23 V *vs.* RHE.

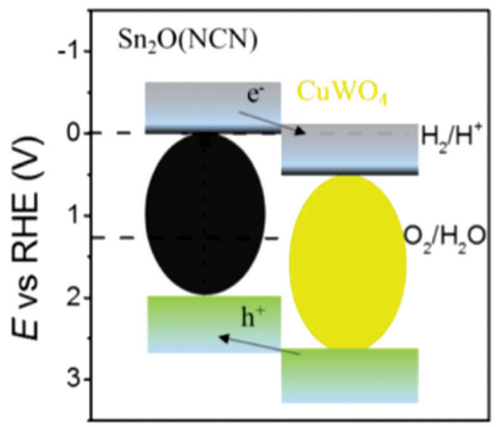

Fig. 12 Energy band diagram of the heterojunction $CuWO_4/Sn_2O$ (NCN).

Conclusions

We have investigated the photochemical properties of Sn_2O (NCN) and showed that this n-type semiconductor can be successfully coupled to $CuWO_4$ thin film photoanodes. Sn_2O (NCN) exhibits a flat-band potential of approx. −0.03 V and as such, the position of the valence band edge would be suitable for photochemical water oxidation. During PEC water oxidation in phosphate buffer electrolyte Sn_2O(NCN) undergoes an *in situ* transformation to a core–shell structure; maintaining a semiconducting core while forming an electrocatalytically-active $SnPO_x$ shell. The obtained composite $CuWO_4/Sn_2O$ (NCN)@$SnPO_x$ photoanodes display a synergetic effect between its constituents during the PEC water oxidation, which shows up in an upsurge of photocurrent from 32 μA cm^{-2} to 59 μA cm^{-2} at 1.23 V *vs.* RHE at pH 7.0 under simulated AM 1.5G illumination. This is due to improved charge carrier separation and augmented hole collection efficiency. Our study demonstrates that mixed-anion compounds containing an oxidic and carbodiimide anion are potential materials for photochemical oxidation reactions, while at the same time, the surface can be electrochemically activated into a catalytically-active form.

Conflicts of interest

There are no conflicts to declare.

Acknowledgements

Zh. C. would like to thank the China Scholarship Council for a PhD scholarship. We thank Ulrich Simon for access to electron microscopy facilities, Birgit Hahn for SEM analysis, and Marek Drozdek for performing XPS, and Istvan-Zoltan Jenei for fruitful discussion. A. S. thank the Fonds der Chemischen Industrie (FCI) and Stockholm University for financial support. The XPS measurements were carried out with the equipment purchased with the financial support of the European Regional Development Fund in the framework of the Polish Innovation Operational Program (contract no. POIG.02.01.00-12-023/08).

References

1 J. P. Holdren, *Science*, 2007, **315**, 737.
2 (*a*) N. S. Lewis, *Nat. Nanotechnol.*, 2016, **11**, 1010–1019; (*b*) M. Grätzel, *Nature*, 2001, **414**, 338–344; (*c*) Z. Ma, T. Thersleff, A. L. Görne, N. Cordes, Y. Liu, S. Jakobi, A. Rokicinska, Z. G. Schichtl, R. H. Coridan, P. Kuśtrowski,

This article is licensed under a Creative Commons Attribution 3.0 Unported Licence.

W. Schnick, R. Dronskowski and A. Slabon, *ACS Appl. Mater. Interfaces*, 2019, **11**, 19077–19086.
3 K. Sivula and R. van de Krol, *Nat. Rev. Mater.*, 2016, **1**, 15010.
4 A. Fujishima and K. Honda, *Nature*, 1972, **238**, 37–38.
5 (*a*) Z. Wang, C. Li and K. Domen, *Chem. Soc. Rev.*, 2019, **48**, 2109–2125; (*b*) C. Jiang, S. J. A. Moniz, A. Wang, T. Zhang and J. Tang, *Chem. Soc. Rev.*, 2017, **46**, 4645–4660; (*c*) H. S. Han, S. Shin, D. H. Kim, I. J. Park, J. S. Kim, P. S. Huang, J. K. Lee, I. S. Cho and X. Zheng, *Energy Environ. Sci.*, 2018, **11**, 1299–1306; (*d*) T. R. Kuo, H. J. Liao, Y. T. Chen, C. Y. Wei, C. C. Chang, Y. C. Chen, Y. H. Chang, J. C. Lin, Y. C. Lee, C. Y. Wenand and S. S. Li, *Green Chem.*, 2018, **20**, 1640–1647.
6 (*a*) D. K. Lee, D. Lee, M. A. Lumley and K. S. Choi, *Chem. Soc. Rev.*, 2019, **48**, 2126–2157; (*b*) J. H. Kim and J. S. Lee, *Adv. Mater.*, 2019, **31**, 1806938.
7 (*a*) K. Maeda, K. Teramura, D. Lu, T. Takata, N. Saito, Y. Inoue and K. Domen, *Nature*, 2006, **440**, 295; (*b*) N. S. Lewis, *Science*, 2007, **315**, 798; (*c*) M. Ertl, Z. Ma, T. Thersleff, P. Lyu, S. Huettner, P. Nachtigall, J. Breu and A. Slabon, *Inorg. Chem.*, 2019, **58**, 9655–9662.
8 (*a*) M. Davi, A. Drichel, M. Mann, T. Scholz, F. Schrader, A. Rokicinska, P. Kuśtrowski, R. Dronskowski and A. Slabon, *J. Phys. Chem. C*, 2017, **121**, 26265–26274; (*b*) M. Davi, M. Mann, Z. Ma, F. Schrader, A. Drichel, S. Budnyk, A. Rokicinska, P. Kuśtrowski, R. Dronskowski and A. Slabon, *Langmuir*, 2018, **34**, 3845–3852; (*c*) M. Davi, F. Schrader, T. Scholz, Z. Ma, A. Rokicinska, R. Dronskowski, P. Kuśtrowski and A. Slabon, *ACS Appl. Nano Mater.*, 2018, **1**, 869–876; (*d*) M. Davi, G. Ogutu, F. Schrader, A. Rokicinska, P. Kuśtrowski and A. Slabon, *Eur. J. Inorg. Chem.*, 2017, **37**, 4267–4274.
9 (*a*) J. E. Yourey and B. M. Bartlett, *J. Mater. Chem.*, 2011, **21**, 7651–7660; (*b*) V. Leute, *Z. Phys. Chem.*, 1966, **48**, 319–339.
10 Z. Ma, O. Linnenberg, A. Rokicinska, P. Kuśtrowski and A. Slabon, *J. Phys. Chem. C*, 2018, **122**, 19281–19288.
11 (*a*) X. Zhou, R. Liu, K. Sun, K. M. Papadantonakis, B. S. Brunschwig and N. S. Lewis, *Energy Environ. Sci.*, 2016, **9**, 892–897; (*b*) Y. Gao, O. Zandi and T. W. Hamann, *J. Mater. Chem. A*, 2016, **4**, 2826–2830; (*c*) X. Zhou, R. Liu, K. Sun, D. Friedrich, M. T. McDowell, F. Yang, S. T. Omelchenko, F. H. Saadi, A. C. Nielander, S. Yalamanchili, K. M. Papadantonakis, B. S. Brunschwig and N. S. Lewis, *Energy Environ. Sci.*, 2015, **8**, 2644–2649.
12 D. Bohra and W. A. Smith, *Phys. Chem. Chem. Phys.*, 2015, **17**, 9857–9866.
13 (*a*) J. E. Yourey, K. J. Pyper, J. B. Kurtz and B. M. Bartlett, *J. Phys. Chem. C*, 2013, **117**, 8708–8718; (*b*) C. R. Lhermitte and B. M. Bartlett, *Acc. Chem. Res.*, 2016, **49**, 1121–1129.
14 J. E. Yourey, J. B. Kurtz and B. M. Bartlett, *Inorg. Chem.*, 2012, **51**, 10394–10401.
15 J. C. Hill, Y. Ping, G. A. Galli and K. S. Choi, *Energy Environ. Sci.*, 2013, **6**, 2440–2446.
16 H. Zhang, P. Yilmaz, J. O. Ansari, F. F. Khan, R. Binions, S. Krause and S. Dunn, *J. Mater. Chem. A*, 2015, **3**, 9638–9644.
17 M. Valenti, D. Dolat, G. Biskos, A. Schmidt-Ott and W. A. Smith, *J. Phys. Chem. C*, 2015, **119**, 2096–2104.
18 Y. Tang, N. Rong, F. Liu, M. Chu, H. Dong, Y. Zhang and P. Xiao, *Appl. Surf. Sci.*, 2016, **361**, 133–140.
19 J. Chouvin, C. Branci, J. Sarradin, J. Olivier-Fourcade, J. C. Jumas, B. Simon and P. Biensan, *J. Power Sources*, 1999, **81**, 277–281.
20 M. T. Sougrati, J. J. Arayamparambil, X. Liu, M. Mann, A. Slabon, L. Stievano and R. Dronskowski, *Dalton Trans.*, 2018, **47**, 10827.
21 A. Eguia-Barrio, E. Castillo-Martinez, X. Liu, R. Dronskowski, M. Armand and T. Rojo, *J. Mater. Chem. A*, 2016, **4**, 1608–1611.
22 H. D. Schädler, L. Jäger and I. Senf, *Z. Anorg. Allg. Chem.*, 1993, **619**, 1115–1120.
23 K. Dolabdjian, A. L. Görne, R. Dronskowski, M. Ströbele and H. J. Meyer, *Dalton Trans.*, 2018, **47**, 13378–13383.
24 J. P. Allen, D. O. Scanlon, L. F. J. Piper and G. W. Watson, *J. Mater. Chem. C*, 2013, **1**, 8194–8208.
25 M. Neukirch, S. Tragl and H. J. Meyer, *Inorg. Chem.*, 2006, **45**, 8188–8193.
26 X. Liu, R. Dronskowski, R. Glaum and A. L. Tchougréeff, *Z. Anorg. Allg. Chem.*, 2010, **636**, 343–348.
27 (*a*) J. P. Allen, D. O. Scanlon, L. F. J. Piper and G. W. Watson, *J. Mater. Chem. C*, 2013, **1**, 8194–8208; (*b*) M. Manikandan, T. Tanabe, P. Li, S. Ueda, G. V. Ramesh, R. Kodiyath, J. Wang, T. Hara, A. Dakshanamoorthy, S. Ishihara, K. Ariga, J. Ye, N. Umezawa and H. Abe, *ACS Appl. Mater. Interfaces*, 2014, **6**, 3790–3793; (*c*) S. Kaizra, B. Bellal, Y. Louafi and M. Trari, *J. Saudi Chem. Soc.*, 2018, **22**, 76–83; (*d*) W. Xia, H. Wang, X. Zeng, J. Han, J. Zhu, M. Zhou and S. Wu, *CrystEngComm*, 2014, **16**, 6841–6847; (*e*) M. Aslam, M. T. Qamar, S. Ali, A. U. Rehman, M. T. Soomro, I. Ahmed, I. M. I. Ismail and A. Hameed, *J. Environ. Manage.*, 2018, **217**, 805–814; (*f*) L. Yang, J. Huang, L. Shi, L. Cao, W. Zhou, K. Chang, X. Meng, G. Liu, Y. Jie and J. Ye, *Nano Energy*, 2017, **36**, 331–340; (*g*) Y. Ogo, H. Hiramatsu, K. Nomura, H. Yanagi, T. Kamiya, M. Hirano and H. Hosono, *Appl. Phys. Lett.*, 2008, **93**, 032113.
28 Q. Hou, M. Zhen, L. Liu, Y. Chen, F. Huang, S. Zhang, W. Li and M. Ju, *Appl. Catal., B*, 2018, **224**, 183–193.
29 R. J. Müller, I. Kuznetsov, Y. Arbelo, M. Trottmann, C. S. Menoni, J. J. Rocca, G. R. Patzke and D. Bleiner, *Anal. Chem.*, 2018, **90**, 9234–9240.

 This journal is © The Royal Society of Chemistry 2020